IEEE Open Journal of
Antennas and Propagation

Received 28 May 2020; revised 4 July 2020; accepted 6 July 2020. Date of publication 9 July 2020; date of current version 31 July 2020.

Digital Object Identifier 10.1109/OJAP.2020.3008292

Time Domain Characteristic Mode Analysis for Transmission Problems

QI WU (Member, IEEE), AND ZHONGKUI WEN

School of Electronic and Information Engineering, Beihang University, Beijing 100191, China

CORRESPONDING AUTHOR: Q. WU (e-mail: qwu@buaa.edu.cn)

This work was supported in part by the National Natural Science Foundation of China under Grant 61971018.

ABSTRACT Characteristic mode analysis (CMA) is based on time-harmonic electromagnetics and applied mostly in frequency domain. In this paper, CMA is extended to time domain (TD) for transmission problems. Based on the modal self- and mutual-admittance of two-port systems, the modal TD response is obtained using inverse fast Fourier transform, extrapolation and Hilbert transform. TD-CMA represents modal impulse response on specified ports, and impulse response of the system is the linear superposition of the modal ones. Numerical examples are provided to explain this new concept. For a pair of parallel wires, the calculated TD-CMA is alike the common and differential modes. For a pair of dipoles, TD-CMA can be divided into strong and weak coupling modes according to their magnitudes. The strong coupling modes are due to the pulse radiation and oscillations at dipole tips and feedings. Time delay paths are clearly observed in the near field but are not discernable in the intermediate field. This shows different coupling mechanisms for the two cases. TD-CMA expands research field of CMA and may find applications for analyzing transient behaviors of microwave systems.

INDEX TERMS Characteristic modes, extrapolation, Fourier transform, modal admittance, time domain.

I. INTRODUCTION

CHARACTERISTIC mode analysis (CMA) attracts extensive attentions for guiding the antenna design, mutual coupling suppression, radiation pattern synthesis, and other emerging applications [1]–[5]. Theory of characteristic modes (TCM) was established in the frequency domain, i.e., the time-harmonic framework [6]–[9]. The eigenvalues and eigencurrents are computed at each single frequency, and a broadband response is obtained by proper mode tracking [10], [11]. Therefore, very few works have considered the modal behaviors in time domain. Nevertheless, some pioneering works tried to combine the CMA and finite-difference time-domain (FDTD) method for computing the eigenvalues and eigencurrents. Electric field with a random spatial distribution is first assumed in FDTD as the initial excitation, and then the electric and magnetic fields in time domain are calculated through time marching [12], [13]. The eigencurrents are calculated by discrete Fourier transform (DFT) of the surface currents stored in each time step. Main advantage of this method is to calculate the eigenvalues and eigencurrents in a large frequency band from a single FDTD run. However, this method is only valid when one single mode dominates at resonance and the computation sometimes fails due to poorly randomized initial fields at zero time. Those drawbacks make this method less useful for realistic problems.

Recently, a new CMA framework in the time domain was proposed for transmission and coupling problems [14], [15], namely time domain CMA (TD-CMA). TD-CMA of a two-port system is based on the modal admittance (MA) that is related to eigencurrents and eigenvalues of the system. Different from the radiation problems, specified excitation ports are required for the signal transmission problems. MA is computed in a large frequency band and its time domain response is obtained by the inverse fast Fourier transformation (IFFT). The modal impulse responses of the pre-defined ports are important for TD-CMA, as they can show how one mode affects the pulse transmission between the two ports. In addition, modal impulse responses can depict the reflections and oscillations of the pulses within the radiators. It is noted that TD analyses of radiators, scatterers and mutual couplings between antennas

have a long history for theoretical or application-oriented purposes [16]–[18].

Although the idea seems to be easily implemented, several issues need to be solved for accurate TD-CMA. Theoretically, IFFT requires the response in the entire frequency spectrum including the DC frequency. However, most CMA codes have a limited computational bandwidth due to known issues such as numerical breakdown in low frequency range and insufficient mesh density in high frequency range as discussed in [11], [19]. Hence, an extrapolation algorithm is adopted to calculate CMA data in low frequency range till the DC frequency [20]. We also try to extrapolate CMA data in high frequency range to improve the time resolution of the TD-CMA. Furthermore, the discrete Hilbert transformation (DHT) is utilized to ensure the causality and the Kaiser Window function is used to suppress the ripples of TD-CMA [21]. Through a series of treatments, TD-CMA of different systems can be accurately calculated and its physical meanings are explained through examples.

The remaining parts of this paper are organized as follows. A summary of CMA and modal admittance in frequency domain are given in Section II. Theory and computation of TD-CMA are also provided in Section II. Dual-wire transmission lines are analyzed in Section III. Near- and intermediate-field mutual couplings between two dipoles are examined in Section IV. Section V discusses TD-CMA of wireless power transfer (WPT) system. This paper is concluded in Section VI.

II. CMA IN THE FREQUENCY AND TIME DOMAINS

A. MODAL ADMITTANCE OF TWO-PORT SYSTEMS

For a two-port system with radiating structures, such as open transmission lines and dual-antenna system, mutual admittance is defined at the two feeding ports in the framework of CMA as follows. The whole system is treated as one structure, meshed with triangular surface elements, and analyzed using MoM with Rao-Wilton-Glisson (RWG) basis and testing functions. After computing the eigencurrents and eigenvalues, the modal self admittance (MSA) and modal mutual admittance (MMA) of the two ports can be obtained [2]. For instance, the MMA reads

$$Y_{21}(j\omega) = \frac{I_2}{V_1} = \sum_{n=1}^{\infty} Y_{21}^n(j\omega) = \sum_{n=1}^{\infty} \frac{I_n(p, j\omega) I_n(q, j\omega) l_p l_q}{1 + j\lambda_n(j\omega)}, \tag{1}$$

where $Y_{21}^n(j\omega)$ is the nth order MMA of ports 1 and 2. The delta-gap voltage V_1 is applied at port 1 with edge index p and length l_p (dimensions in m), and the induced current I_2 at port 2 with edge index q and length l_q is decomposed into modes. $I_n(p, j\omega)$ and $I_n(q, j\omega)$ (dimensions in A/m) are coefficients of the basis function for $\mathbf{J}_n$. MSA and MMA can be calculated in a wide frequency range by proper mode tracking. The data in frequency domain can be transformed to time domain and we get the so-called TD-CMA for transmission problems.

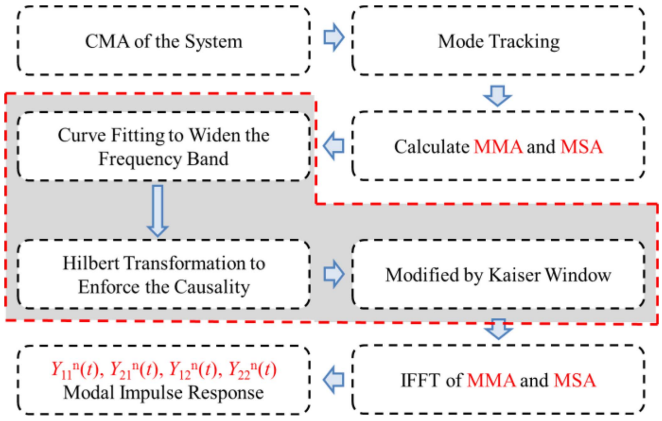

FIGURE 1. Computational procedures of TD-CMA for transmission problems. The steps in the gray area are necessary for complicated problems like near-field coupling and may be skipped for others. Curve fitting is optional to widen the computational bandwidth of modal admittance, and DHT is used to ensure the causality. The Kaiser window can suppress the ripples of the computed curves.

B. TIME DOMAIN RESPONSE

MSA and MMA are functions of frequency and they can be denoted as $Y_{11}^n(j\omega)$ and $Y_{21}^n(j\omega)$, respectively. According to (1), $Y_{21}(j\omega)$ can be expressed into a linear superposition of $Y_{21}^n(j\omega)$, and thus its IFFT $Y_{21}(t)$ can be denoted as the superposition of $Y_{21}^n(t)$ due to the linear feature of IFFT. In this sense, $Y_{21}^n(t)$ is the nth order modal impulse response of the system for transmission problems.

Calculation of TD-CMA is based on IFFT of MA and some works need to be done because IFFT requires the frequency response in the entire spectrum. However, general mode tracking routine provides only band-limited data, which may be insufficient for accurate TD analysis. In this paper, a set of computation procedures for TD-CMA are proposed as shown in Fig. 1.

It is important to understand the relationship of the frequency data and recovered time curves. We assume that the MMA is calculated from $f_{\min}$ (and extrapolated to DC) to $f_{\max}$ with a uniform frequency step f_{step}. The largest calculation frequency $f_{\max}$ determines the resolution (time step) in time domain, i.e., $t_{step} = 1/f_{\max}$. The frequency step, on the other hand, restrains the maximum time duration as $t_{\max} = 1/f_{step}$. The resolution and duration are important time-domain parameters for depicting narrow pulses and late-time signal, respectively. Finally, the impulse response of a general two-port system is divided into linear superposition of modal impulse responses as

$$Y_{21}(t) = \sum_{n=1}^{\infty} Y_{21}^n(t) = \sum_{n=1}^{\infty} F^{-1}\left[Y_{21}^n(j\omega)\right] \tag{2}$$

Time domain curves of MSA are obtained in a similar way. The eigenvalues and eigencurrents established in frequency domain are solely determined by the structural geometry at one single frequency. Contrarily, TD-CMA for transmission problems is related to the geometry, feeding positions and

the data in the entire frequency spectrum. Therefore, TD-CMA can reflect how one mode attributes to the fundamental responses of the system in the linear system sense.

The procedures in the gray area are optional, in which the extrapolation, DHT and Kaiser window function is applied to improve the computation. One may drop those procedures for simple problems or using more accurate CMA solvers in future.

First, we introduce the DHT procedure. Wireless and wired transmissions are causal, which ensures that the output current depends only on the past and current excitation. The causality ensures the computation of correct time delays. The modal solutions are causal since no output would appear before the excitation ever applies. Take the MMA as an example, the DHT is a useful approach to enforce the causality as

$$\mathrm{Im}\left[Y_{21}^{n}(j\omega)\right] = H\left\{\mathrm{Re}\left[Y_{21}^{n}(j\omega)\right]\right\}, \tag{3}$$

The DHT is necessary for TD-CMA because numerical error of CMA is somewhat larger than that of MoM with the same mesh. Especially, convergence of the imaginary part of eigencurrents is poor, whereas the real part converges rapidly as discussed in [23]. Therefore, only the real parts of MMA are reserved and the imaginary parts are calculated by (3) to ensure the causality.

Mode tracking sometimes fails in low frequency range due to the existence of degenerated modes or numerical errors. As a result, the lower frequency $f_{\min}$ cannot reach the desirable one, i.e., f_{step}. Instead, we can extrapolate $f_{\min}$ to the DC frequency by setting the real part an even function such as [18]

$$\mathrm{Re}\left[Y_{21}^{n}(j\omega)\right] = e_1\omega^2 + e_2 \tag{4}$$

where e_1 and e_2 are the fitting coefficients. The DC value e_2 is obtained by theoretical analysis. Take dual-wire transmission line with a slit and antenna problems as an example, e_2 is zero because no signals are transmitted at DC frequency. e_1 is then obtained through the full-wave result at the lower frequency $f_{\min}$ and extrapolate the MMA to DC using (4).

To extend the analysis to higher frequency range, one may extrapolate the MMA using the sum of sine and cosine series as

$$\mathrm{Re}\left[Y_{21}^{n}(j\omega)\right] = \sum_{n=1}^{N}\left(\frac{a_n\cos(b_n\omega)}{g_n\omega + h_n} + \frac{c_n\sin(d_n\omega)}{l_n\omega + m_n}\right), \tag{5}$$

where a, b, c, d, g, h, l, m are the coefficients to be determined.

Since envelope of the MMA decays slowly with the frequency, a first-order polynomial is regarded as a denominator in (5).

The IFFT to time domain in (3) may yield many ripples due to the abrupt truncation of frequency domain data (equivalent to a rectangular window). In this paper, a Kaiser window is used to reduce the frequency leakage for alleviating the ripples as [24]

$$K(n) = \begin{cases} \dfrac{I_0\left[\beta\left(1-\left[(n-\alpha)/\alpha\right]^2\right)^{1/2}\right]}{I_0(\beta)} & 0 \le n \le M \\ 0 & others \end{cases} \tag{6}$$

where $M = f_{\max}/f_{step}$, $\alpha = M/2$ and I_0 is the zeroth order modified Bessel function of the first kind. β is a coefficient that controls the shape of Kaiser window. Obviously, $M+1$ is the number of frequency points used for computing the MMA.

Computational complexity of TD-CMA is similar as that of CMA in frequency domain. The mostly time-consuming parts are the fill-up of impedance matrix *[Z]* and the eigenvalue decomposition of *[Z]*. The extrapolation, DHT, Kaiser window, and IFFT are usually fast. However, CMA consumes more time than full-wave solution, especially for large platforms [4], [25].

C. COMPARISON WITH TIME-DOMAIN REFLECTOMETRY

Time-domain reflectometry (TDR) is a well-known method that utilizes the impulse response of transmission lines. One port of the transmission line is usually terminated by a matched load and a short pulse is injected to the other port. Wave reflections happen when the pulse encounters discontinuities along the transmission line, and the discontinuities are located and characterized by measuring the magnitude, wave form, and time delay of the reflected pulses [26]–[28].

TDR utilizes the impulse response that is obtained by IFT of the S parameters. On the other hand, TD-CMA is based on the modal admittance in (1), i.e., mode decomposition of the Y parameters. As S parameters can be transformed into the Y parameters using $[Y(j\omega)] = ([I] + [S(j\omega)])^{-1}([I] - [S(j\omega)])$ ($[I]$ is the identity matrix), TD-CMA is essentially the mode decomposition of TDR.

TDR is physically implemented by instruments like the pulse generator and oscilloscope, which is very useful for locating faults in long transmission lines. Contrarily, TD-CMA is a tool for transmission problems, which is useful for understanding the underlined physics and optimizing them through proper mode control. TD-CMA is general and it is applicable for transformers, which is out of the scope of TDR [26]–[28]. However, TD-CMA requires a mode decomposition, which adds somewhat computational complexity and error. Hence, TDR has a better time resolution than that of TD-CMA.

III. TD-CMA OF DUAL-WIRE TRANSMISSION LINES

CMA is suitable to expand electromagnetic fields outside a metallic structure but it is seldom used for transmission lines. However, open transmission lines such as dual-wire, microstrip line, and slot line can produce somewhat radiated emission (RE) in the high frequency range [29]. Therefore, it is interesting to compare characteristic modes and guided modes. Dual-wire is a type of transverse electromagnetic (TEM) transmission line operating from DC to microwave bands, and its characteristics have been well

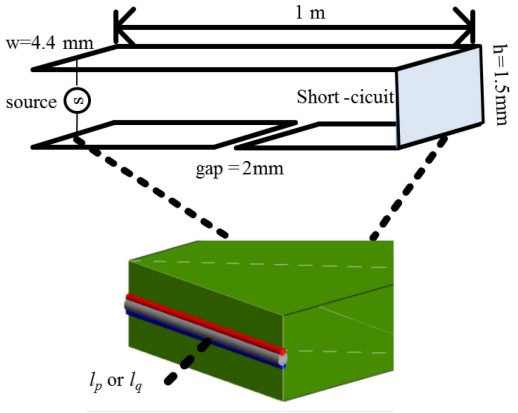

FIGURE 2. Structural configuration of the dual-wire transmission line with a split. A voltage source is placed at port 1 and a short-circuit plate terminates port 2.

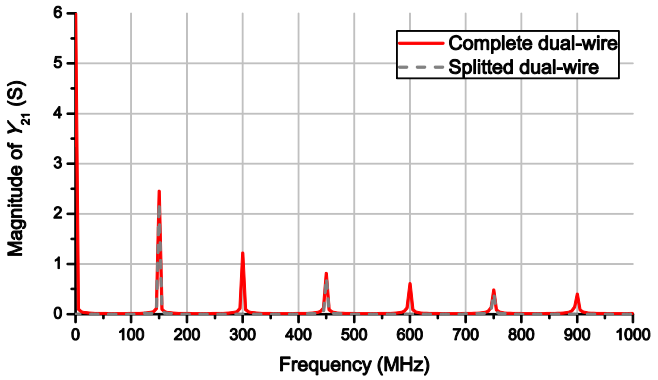

FIGURE 3. Y_{21} parameters of the complete and splitted dual-wire transmission lines. The value at DC is calculated analytically and it equals to zero for the split one.

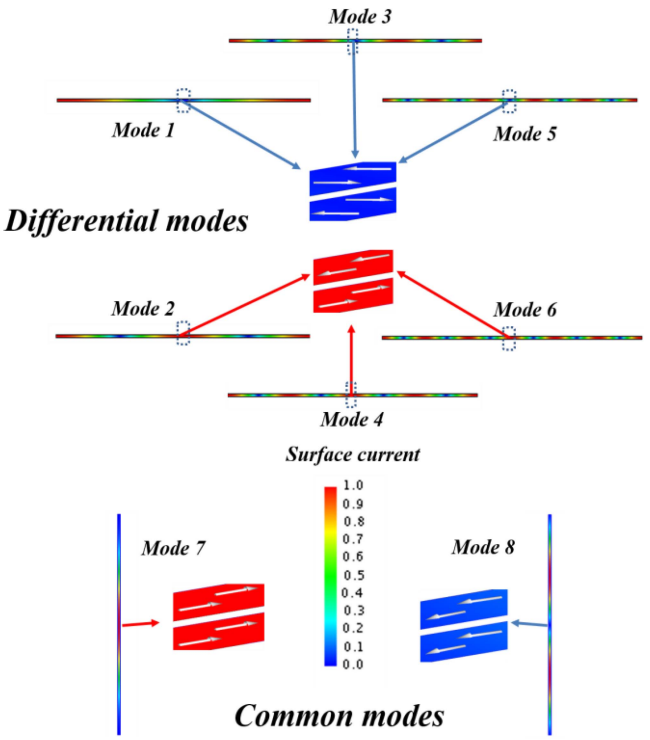

FIGURE 4. Eigencurrent distributions of the differential modes (signal transmission) and common modes (radiated emission) for the complete dual wire structure.

investigated and understood [29]. Therefore, it is ideal for benchmarking the presented TD-CMA algorithm.

Previously, a dual-wire transmission line was analyzed using the TD-CMA approach [15]. In this paper, a split is added to the structure for enhancing common mode (CM) currents, which is a common fault for producing extra RE [29]. The split alternates the frequency response significantly, and one may observe the modes contributing differently to the transmission and emission. Structural configuration of the dual-wire is illustrated in Fig. 2. In the MoM model, the dual-wire is narrow rectangular plates with zero thickness. Its length is 1 meter and width of the two wires is 4.4 mm. The gap of the dual-wires is 1.5 mm and it achieves a characteristic impedance of 50 Ω. The averaged mesh length is 5 mm in MoM, which results in 840 and 839 unknowns for the complete and splitted lines, respectively. A voltage source is placed at port 1 and port 2 is terminated by a short-circuit plate. Y_{21} of the complete and splitted transmission lines are calculated using MoM and the results with a step of 5 MHz are shown in Fig. 3. Value of Y_{21} at DC frequency is equivalent to the inverse of wire resistance, which is calculated from conductivity of copper wires. For the ideal symmetric dual-wire structure, it is unnecessary to take more efforts on widening the frequency band. A deduction is that MMA of differential mode (DM) concentrates only at one frequency with small out-of-band response and MMA of CM is close to zero in the frequency range of interest.

For the complete dual-wire, transmission peaks of Y_{21} have a period of 150 MHz as expected. There are six transmission peaks in the frequency up to 1000 MHz, which are significant modes [15] and their eigencurrent distributions at 150 MHz are illustrated in Fig. 4. It is seen that they have the same amplitude but reversed phase, which are DM for signal transmission. CM with the same amplitude and phase is also observed. Although the dual-wire is terminated at the two ends like a loop, eigencurrents look alike the case without any termination. The reason is that the gap between the dual-wire is only 1.5 mm, and the long wire (1000 mm) determines the lower order modes. Eigencurrents of DM abide the cosine-type function, whose electrical lengths are exactly multiple integers of one half length of the transmission line. However, eigencurrents of CM have nulls at the terminals of transmission line.

Based on the presented analysis, full-band MMA data of DM and CM are obtained by conjugation and extrapolation towards negative frequency. By using IFFT, $Y_{21}^{n}(t)$ of the dual-wire are obtained, which are cosine-type functions and the time period corresponds to the reverse of the transmission peak frequencies. Besides, DC components ought to be compensated on MMA and a constant C represents the residue in time domain. Finally, a closed-form expression of

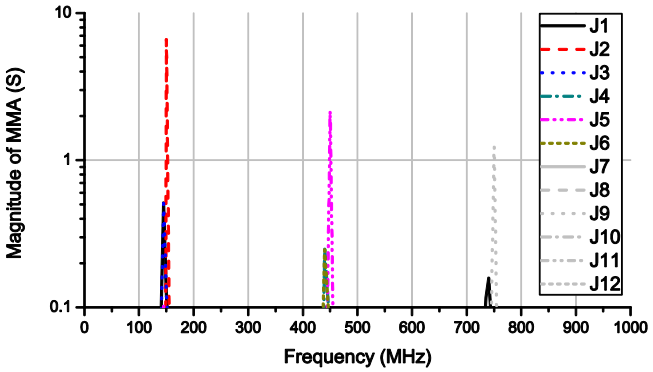

FIGURE 5. MMA of the dual-wire transmission line with a split.

DMs is given as

$$Y_{21}^{n}(t) = A_n \cos\left[(f_0 + kf_{s1})(t - t_0) + \phi_n\right] + C_n, \qquad (7)$$

where $k = 1, 2, 3, 4 \cdots$. belongs to positive integers. Both f_0 and f_{s1} are 150 MHz. A_n is magnitude of the transmission peaks in the frequency domain and C_n is the residue DC component. ϕ_n denotes the initial phase and t_0 is the time delay of the dual-wire. CM current is very close to zero for ideal dual-wire structure.

TD-CMA is also applied to the spitted dual-wire structure in Fig. 2, which can help understanding its transmission properties. The split is placed at the center of the line with a gap of 2 mm. Y_{21} and MMA of the splitted model are shown in Figs. 3 and 5, respectively. Transmission peaks of Y_{21} and MMA has a period of 300 MHz in the frequency domain. It is seen that three DMs (modes 2, 4 and 6) are unable to transmit to the other terminal, because their eigencurrents have peak value at the split as shown in Fig. 4 and hence they are somewhat suppressed.

Eigencurrents of modes 1, 3 and 5 have nulls at the split and they are hardly affected. Therefore, the modal impulse response of the dual-wire line with a split is similar to (7) and read

$$Y_{21}^{n}(t) = A_n \cos\left[(f_0 + kf_{s2})(t - t_0) + \phi_n\right]. \qquad (8)$$

where f_{s2} is 300MHz and C_n is removed as the transmission at DC frequency is blocked by the split. Also, it can be found that several small pulses appear in Fig. 5 as the split damages the symmetry of dual-wire, introduce CMs and produce RE.

Based on the presented method, time-domain response of the dual-wire with a split is shown in Fig. 6. TDR curve, which is obtained by IFT of Y_{21}, is also provided for comparison. Several transmission delays are clearly seen from the TDR curve, for instance, ct = 1 m, ct = 2 m, etc. The dominate mode J1 predicts those transmission delays but the time resolution is not as good as that of the TDR. Especially, delays of 3 m and 4 m are hardly seen. J2, J3, and J5 yield lossless transmission behaviors, which belong to DMs and can be described by (9). J4 and J6 are CMs, in which the radiation loss is significant and hence they yield lossy

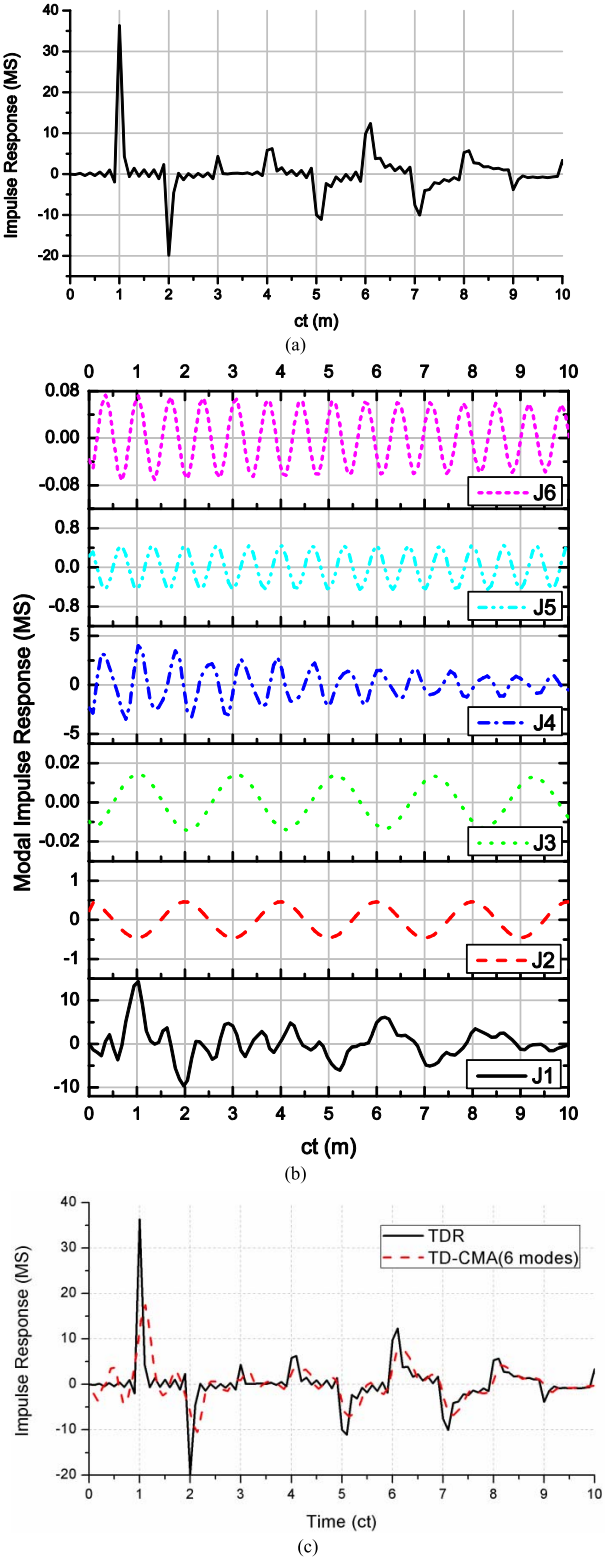

FIGURE 6. Time-domain response of the dual-wire with a split: (a) TDR obtained by IFT of Y_{21}, (b) TD-CMA obtained by IFT of MMA, and (c) comparison of the TDR and summation of TD-CMA (with 6 modes).

transmission behaviors. Fig. 6(c) compares the TDR and TD-CMA results (with 6 modes) and the two curves show the same trend and time delays. Magnitude of TDR is

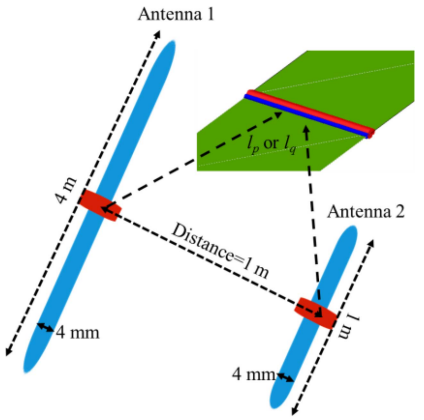

FIGURE 7. Structural configuration of two dipole antennas placed close to each other. The geometry is modeled as rectangle plates with zero thickness.

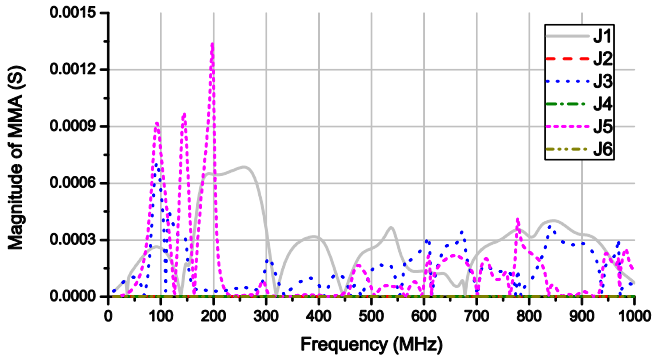

FIGURE 8. Magnitude of MMA for the two dipole antennas. Unlike the dual-wire transmission line, the MMA spans the whole frequency range of interest.

sharper at the reflection points owing to its better time resolution.

IV. MUTUAL COUPLING BETWEEN TWO WIRE ANTENNAS

A. TD-CMA OF NEAR-FIELD MUTUAL COUPLING

Unlike the dual-wire discussed in Section III, more efforts are made to perform the TD-CMA of two dipoles shown in Fig. 7. Especially, if the distance between the two dipoles is short, the frequency domain response is rather complicated and all the components attribute to the TD-CMA. The proposed procedure shown in Fig. 1 is followed for TD-CMA of near-field mutual coupling between two dipoles. The average mesh length is 5 mm and results in 2078 unknowns in MoM. DC values of the Y-parameters and MMA are obtained similarly as dual-wire with a split. The response in the entire frequency spectrum is desirable for computation but it is not possible in practice. The MMA curves are disorganized in a rather wide frequency band as shown in Fig. 8. In addition, the original data of MMA are only available up to 1 GHz, which is insufficient to get good time solution and may results in large ripples and distortions. Therefore, enlarging the frequency band is helpful by a curve fitting algorithm. In order to obtain causal data for IFFT, the real part is selected as the original data for

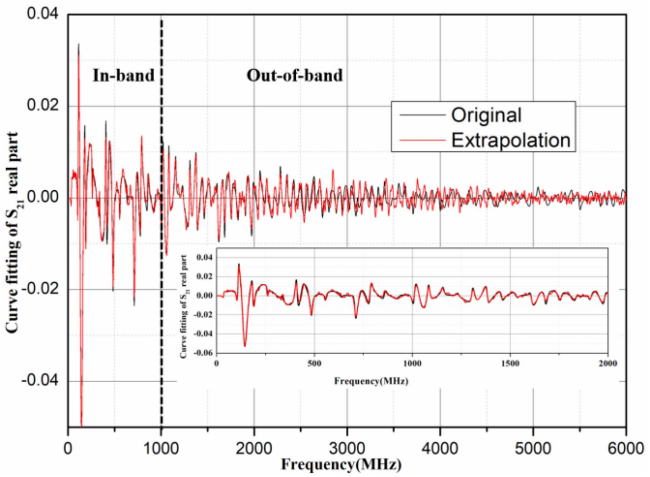

FIGURE 9. The original and curve fitted real parts of S_{21}. The real parts, simulated from 50 MHz to 1 GHz with a step of 1 MHz are regarded as the original data to obtain the analytic expression of sine or cosine types' functions.

curve fitting using (5). Based on our trials, 16 orders of sine or cosine functions are required for this problem. Real parts of S_{21} (10 MHz–1 GHz with a step of 1 MHz) are used for verification. The residual square sum of the curve fitted result is ∼0.002 and the root mean square error is ∼0.001, which are sufficient for computation.

Fig. 9 shows the original and curve-fitting values of the real parts of S_{21} in the frequency range of 0–6 GHz. The data in the frequency range of 0–2 GHz are provided in detail to prove that the fitted data agree with the original ones. Besides, a Kaiser window in (7) is introduced to prevent the effects of spectrum truncation as shown in Fig. 10. The DHT is applied to calculate the imaginary part from the real part of S_{21}. Based on the improved S_{21} data, the impulse response in the time domain is solved using the IFFT. The results using original data within 0–6 GHz (MoM), original data within 0–1 GHz (MoM), and the interpolated data within 0–6 GHz using the original data within 0–1 GHz (MoM) are illustrated in Fig. 10 for comparison.

The measured impulse response of a similar configuration with two monopoles was provided in [16]. The result computed by the original data within 0–6 GHz (MoM) and the one by the interpolation coincide with the measured results [16]. It proves that curve fitting using the cosine and sine series can improve the accuracy of the IFFT using the band-limited S parameters. Similar curve fitting procedure is applied to MMA data. Modal impulse responses of the first six modes are shown in Fig. 11. Magnitudes of the impulse responses for modes 2, 4 and 6 are much smaller than the others, which are regarded as the "weak coupling modes". These modes cannot be excited as the surface current densities have nulls at the feeding points [2]. Modes 1, 3 and 5 make large contributions to mutual coupling and denoted as "strong coupling modes". Time delay of these modes is ∼3.3 ns, which corresponds to 1 meter distance that electromagnetic wave can propagate in this time delay.

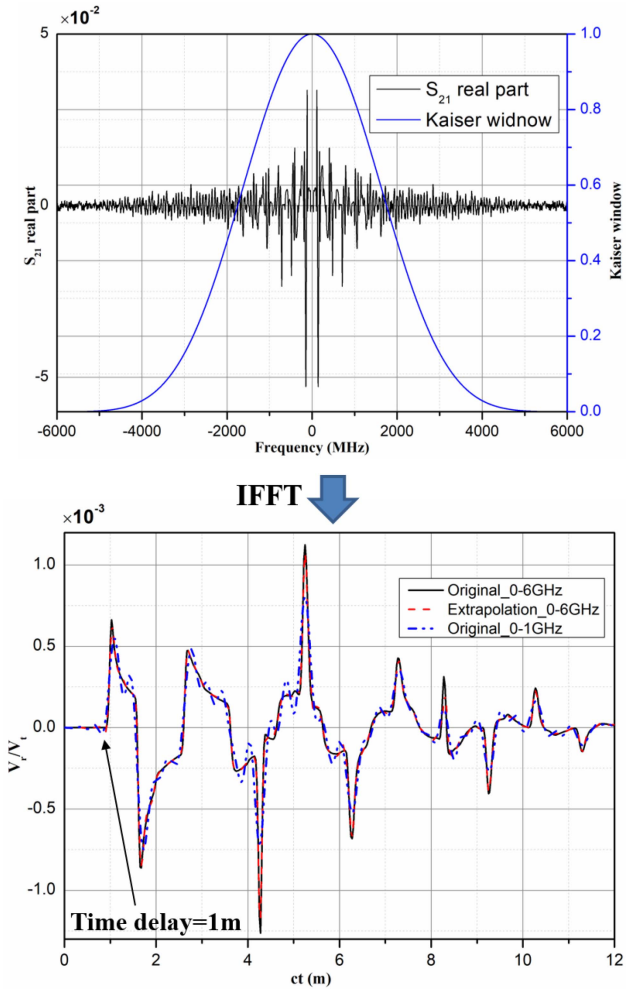

FIGURE 10. A modified IFFT algorithm with the Kaiser window. The ripples and overshoots in the time domain are suppressed by the Kaiser window.

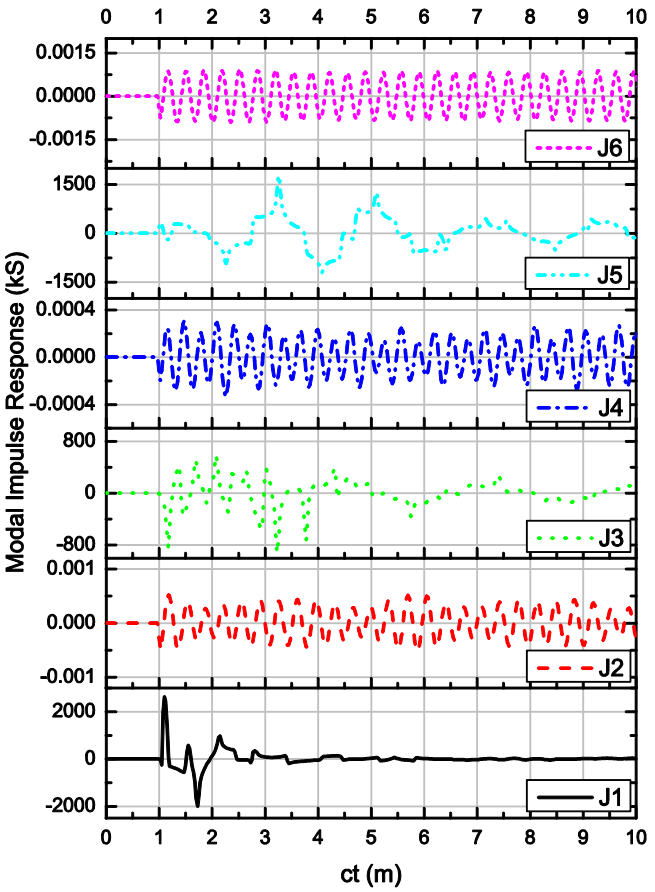

FIGURE 11. The modal impulse responses of the first six modes.

The surface current can be reflected by the end of antenna 1 and introduce a second time radiation. The reflected wave reaches the feeding point and will be reflected again and behave like a second pulse excitation. The reflections at the tips and feeding points behave like pulse oscillations and the energy is coupled to antenna 2 during the oscillations. These phenomena were carefully examined by Sato *et al.*, in which different scenarios were provided to describe possible coupling paths as exemplified in Fig. 12 [16]. In general, those scenarios coincide with the simulated results in Fig. 10 and the measured ones in [16]. Specifically, the scenarios with ct = 1.0 m, ct = 1.62 m, ct = 2.62 m, ct = 4.24 m, and ct = 5.24 m have large impulse magnitude and are easily discernable from Fig. 10.

Other scenarios like ct = 2.0 m and 5.0 m have smaller magnitude, which are more difficult to observe from Fig. 10 or the measured results in [16].

The TD-CMA results shown in Fig. 11 give different physical insights. Modes 1 and 3 have similar curves and the results indicate that they belong to quasi degenerated functional modes [2]. Mode 5 should be the non-functional modes, in which the eigencurrent of antenna 1 has three peaks and two nulls. The time period of oscillations is about 0.5 m, which corresponds to the pulse oscillations on antenna 2. Modes 1 and 3 have a smaller period of oscillations, showing that the coupling is weak owing to wave propagation. In addition J1 contains the information about scenarios of ct = 1.0 m, ct = 1.62 m, and ct = 2.0 m. J3 is the quasi degenerated modes of J1, and hence it has similar path delays but show inversed pulse polarization in the early time. Moreover, J3 depicts the scenario of ct = 2.62 m too, which is not so clear depicted by J1. J5 depicts the mechanisms of ct = 4.24 m and ct = 5.24 m. J2, J4, and J6 are very weak in magnitude and look alike tuned sinuous signals. Based on the presented discussions, it seems that TD-CMA decomposes the coupling mechanisms into modes at the cost of time resolution.

B. TD-CMA OF INTERMEDIATE-FIELD MUTUAL COUPLING

As illustrated in Fig. 13, the distance between the two dipoles increases to 10 m and we regard this as intermediate-field case as the distance is between the inductive and radiative fields. The average mesh length is 5 mm and results in 1038 unknowns in MoM. It is easier to handle the intermediate-field mutual coupling as the curves of Y_{21}

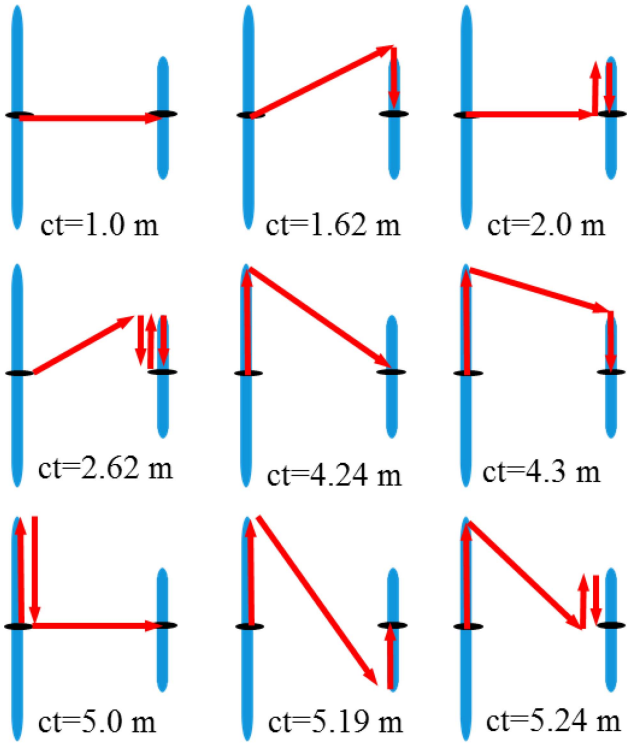

FIGURE 12. Possible coupling mechanisms of the two dipoles.

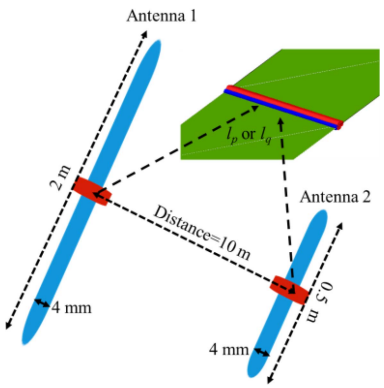

FIGURE 13. Structure of two dipole antennas placed in the intermediate field region.

have fewer variations than the corresponding ones in the near-field. The modal admittance can be computed in the frequency range of 10–3000 MHz with a frequency step of 2.5 MHz as shown in Fig. 14. The frequency response needs to be extrapolated in the low frequency range to DC frequency, but no effort is required to extend the data in the high frequency range. The full-wave data shown in Fig. 14 are processed by the IFFT algorithm to get the time-domain responses. The results of the first six modes are provided in Fig. 15. Similar as the case in the near-field, the modes are divided into the strong and weak coupling ones. Modes 3, 4, 5 and 6 are weak coupling ones due to their small magnitudes. Modes 1 and 2 are strong coupling modes with larger magnitudes. Those modes have several sense pulse trains with a delay about 33 ns (about ct = 10 m),

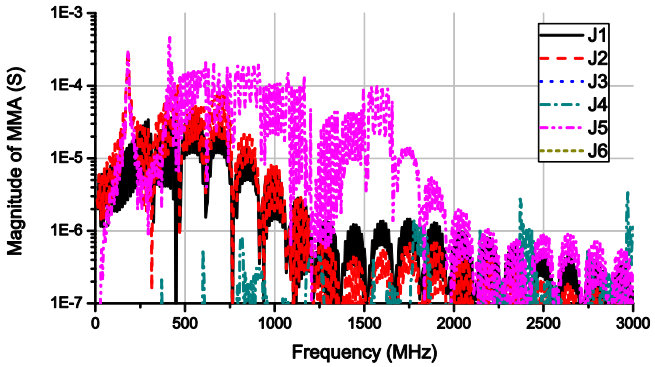

FIGURE 14. MMA of the first six modes of two dipoles placed at the intermediate field. Different from the near-field case, MMA has many discrete pulses.

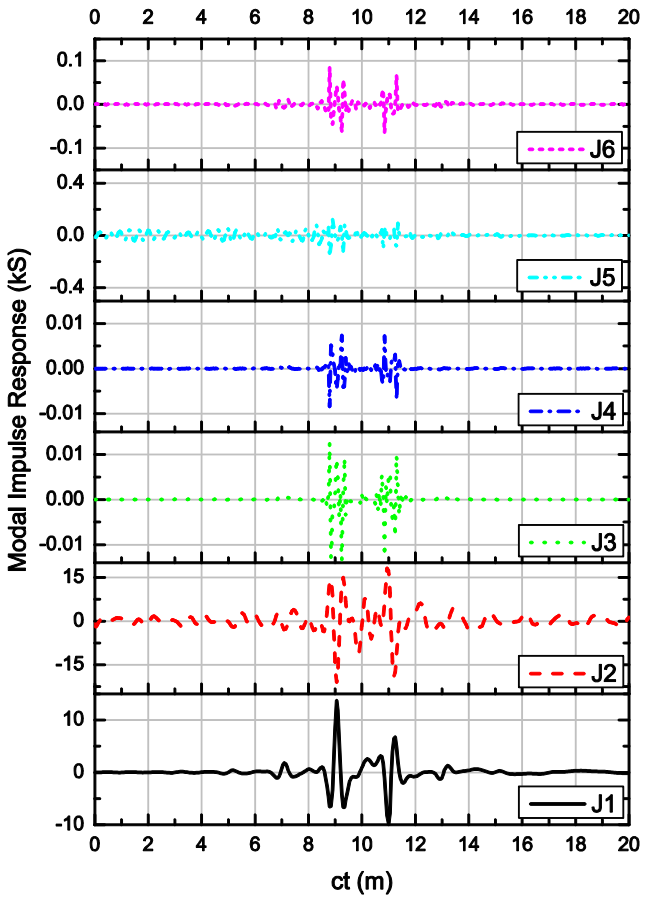

FIGURE 15. The intermediate-field modal impulse responses of the first 6 modes.

which are mainly caused by the reflection and radiation of the reflected waves at the feeding and tips of the dipole, or say the oscillations. The coupling mechanisms illustrated in Fig. 12 are difficult to observe as path delays of different mechanisms are smaller than the distance of the two dipoles. This finding explains different mechanisms for the studied cases: mutual coupling in the intermediate-field is owing to electromagnetic radiation whereas the near-field one is mainly caused by the inductive coupling.

TABLE 1. Correlation factors of the modal impulse responses.

Modes	1	2	3	4	5	6
1	1	0.7233	0.0480	0.0243	0.0014	0.0387
2	0.7233	1	0.0420	0.0194	0.0003	0.0319
3	0.0480	0.0420	1	0.9292	0.1468	0.7989
4	0.0243	0.0194	0.9292	1	0.3529	0.9304
5	0.0014	0.0003	0.1468	0.3529	1	0.4965
6	0.0387	0.0319	0.7989	0.9304	0.4965	1

It is interesting to analyze orthogonality of the modal impulse responses shown in Fig. 15. In the time domain, we can use the correlation factor for this purpose as

$$\rho_{ij} = \max_{\tau} \left\{ \frac{\left| \int Y_{21}^{i}(t) Y_{21}^{j}(t-\tau) dt \right|}{\sqrt{\int \left[Y_{21}^{i}(t) \right]^2 dt} \sqrt{\int \left[Y_{21}^{j}(t) \right]^2 dt}} \right\} \tag{9}$$

As the modal impulse responses in Fig. 15 are a group of time series, the correlation factor can be obtained by simple vector multiplications as shown in Table 1. It is seen that the strong coupling modes, i.e., modes 1, 2 have a large correlation factor and hence they are quasi degenerated modes. Similarly, the weak coupling modes 3 and 4 have a correlation factor close to 1, which indicate that they are the degenerated modes. Moreover, the weak coupling modes 5 and 6 have a correlation factor close to 0.5, and hence they belong to quasi degenerated modes. The correlation factors between the three groups of degenerated modes are very small correlation factors, and hence they are almost independent. From those results, the modal impulse responses seem to be orthogonal to each other except for the quasi degenerated modes. It is slightly different from the characteristic modes in the frequency domain as the degenerated modes are orthogonal as well.

V. POTENTIAL APPLICATIONS OF TD-CMA

This paper introduces the concept and computation of a new CMA tool in the time domain. TD-CMA is potentially useful for understanding the transient behaviors of PEC radiators in broadband communication systems and pulse-based systems. It is also applicable to transmission problems, such as the ones involving transformers those may be difficult for TDR method. Recently, TD-CMA is adopted to analyze a mid-range wireless power transfer (WPT) system as exemplified in Fig. 16. The WPT system consists of two identical helix coils. Each coil is loaded by a shunt capacitor for tuning the resonant frequency [30]. The average mesh size is 7 mm and results in 702 unknowns in MoM. Modal impulse responses of this system are calculated by the proposed method and the results are shown in Fig. 17. For comparison, the impulse response of the WPT system is also calculated and shown in Fig. 17(c). It is seen that it equals to the summation of the modal impulse responses, which verifies the statement in (3).

The impulse response of the WPT system, as shown in Fig. 17, looks like a tuned sinuous signal. On the other hand,

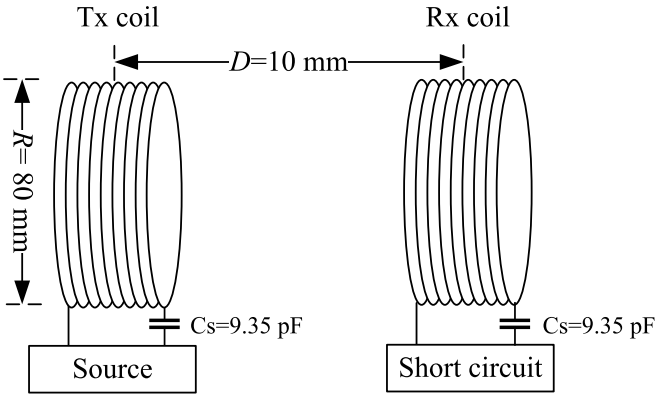

FIGURE 16. Structural parameters of the WPT system.

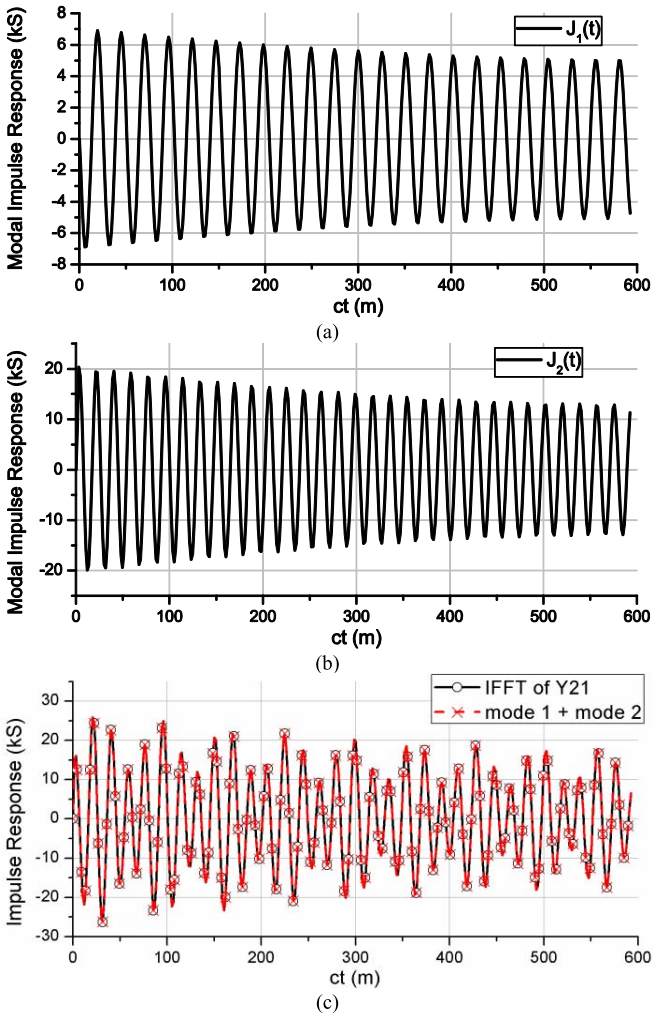

FIGURE 17. Time-domain response of the WPT system: (a) modal impulse response (J1), (b) modal impulse response (J2), and (c) impulse response calculated by the IFT of Y_{21}.

the modal impulse responses are clear to be damped sinuous waves and conform to

$$\mathbf{J}_n(t) = A_n e^{-\alpha_n t} \cos(2\pi f_n t + \varphi_n) \tag{10}$$

where α_n is the time constant and f_n is the resonant frequency of the nth order modal impulse response. A_n and φ_n are the initial amplitude and phase of the nth order mode. TD-CMA shows that the WPT system contains two types of transmission modes when the transmission distance is smaller than diameter of the coil and the two modes tend to be degenerated if the distance is increased [30]. This conclusion coincides with the theory of WPT system, which can be useful for designing active loads for robust power transmission [31].

VI. CONCLUSION

In this paper, a new TD-CMA is proposed for transmission problems. TD-CMA is based on MSA and MMA of a two-port system in frequency domain. A set of algorithms are developed for accurate computation of TD-CMA, including IFFT, DHT, and extrapolation. TD-CMA represents the modal impulse response on specified ports, and the impulse response is linear superposition of the modal ones. As the method is based on full-wave solutions, it is applicable to different structures.

Although TD-CMA is based on the IFFT of CMA results (in frequency domain), it can depict the whole picture instead of discrete resonances. Therefore, TD-CMA contains some useful information about the structure, which may be implicit from chaos-like CMA data in a large bandwidth. In addition, TD-CMA can reveal the propagation mechanisms and indicate possible optimization through mode control. It is also noted that time resolution of TD-CMA deteriorates somehow due to numerical errors of mode decomposition.

For a pair of dipole antennas, TD-CMA can be divided into strong and weak coupling modes according to their magnitudes. The strong coupling modes are due to direct pulse radiation and the reflections and oscillations of the pulse at the dipole tips and feedings. The time delay phenomenon of weak coupling modes is clearly observed in the intermediate-field region only. This shows different coupling mechanisms for the two cases.

TD-CMA is also applied to magnetic resonance based WPT system. It is seen that the modal impulse responses reveal the transmission mechanisms clearly, which may be very difficult for depicting the impulse response like the TDR method.

REFERENCES

[1] M. Cabedo-Fabres, E. Antonino-Daviu, A. Valero-Nogueira, and M. F. Bataller, "The theory of characteristic modes revisited: A contribution to the design of antennas for modern applications," *IEEE Antennas Propag. Mag.*, vol. 49, no. 5, pp. 52–68, Oct. 2007.

[2] Q. Wu, W. Su, Z. Li, and D. Su, "Reduction in out-of-band antenna coupling using characteristic mode analysis," *IEEE Trans. Antennas Propag.*, vol. 64, no. 7, pp. 2732–2742, Jul. 2016.

[3] J. Ethier and D. A. McNamara, "The use of generalized characteristic modes in the design of MIMO antennas," *IEEE Trans. Magn.*, vol. 45, no. 3, pp. 1124–1127, Mar. 2009.

[4] Z. T. Miers and B. K. Lau, "Computational analysis and verifications of the characteristic modes in real materials," *IEEE Trans. Antennas Propag.*, vol. 64, no. 7, pp. 2595–2607, Jul. 2016.

[5] D. Manteufflel and R. Martens, "Compact multimode multielement antenna for indoor UWB massive MIMO," *IEEE Trans. Antennas Propag.*, vol. 64, no. 7, pp. 2689–2697, Jul. 2017.

[6] R. J. Garbacz, "A generalized expansion for radiated and scattered fields," Ph.D. dissertation, Dept. Elect. Eng., Ohio State Univ., Columbus, OH, USA, 1968.

[7] R. F. Harrington and J. R. Mautz, "Theory of characteristic modes for conducting bodies," *IEEE Trans. Antennas Propag.*, vol. 19, no. 5, pp. 622–628, Sep. 1971.

[8] Q. I. Dai, Q. S. Liu, H. U. I. Gan, and W. C. Chew, "Combined field integral equation-based theory of characteristic mode," *IEEE Trans. Antennas Propag.*, vol. 63, no. 9, pp. 3973–3981, Sep. 2015.

[9] L. Guan, Z. He, D. Z. Ding, and R. S. Chen, "Efficient characteristic mode analysis for radiation problems of antenna arrays," *IEEE Trans. Antennas Propag.*, vol. 67, no. 1, pp. 199–206, Jan. 2019.

[10] B. D. Raines and R. G. Rojas, "Wideband characteristic mode tracking," *IEEE Trans. Antennas Propag.*, vol. 60, no. 7, pp. 3537–3541, Jul. 2012.

[11] M. Capek, V. Losenicky, L. Jelinek, and M. Gustafsson, "Validating the characteristic modes solvers," *IEEE Trans. Antennas Propag.*, vol. 65, no. 8, pp. 4134–4145, Aug. 2017.

[12] N. Surittikul and R. G. Rojas, "Analysis of reconfigurable printed antenna using characteristic modes: FDTD approach," in *Proc. IEEE Antennas Propag. Soc. Symp.*, vol. 2. Monterey, CA, USA, 2004, pp. 1808–1811.

[13] N. Surittikul and R. G. Rojas, "Time domain method of characteristic modes for the analysis/design of reconfigurable antennas," in *Proc. IEEE Antennas Propag. Soc. Symp.*, vol. 2B. Washington, DC, USA, 2005, pp. 585–588.

[14] Z. Wen and Q. Wu, "Revisit of signal traces crossing split ground plane using characteristic mode analysis," *Presented at the 6th Asian–Pac. Conf. Antennas Propag. (APCAP)*, Xi'an, China, 2017, pp. 1–3.

[15] Z. Wen and Q. Wu, "Time domain characteristic mode theory for transmission and coupling problems," *Presented in the IEEE Int. Conf. Comput. Electromag. (ICCEM)*, Chengdu, China, 2018, pp. 1–3.

[16] M. Sato, M. Iguchi, and R. Sato, "Transient response of coupled linear dipole antennas," *IEEE Trans. Antennas Propag.*, vol. 32, no. 2, pp. 133–140, Feb. 1984.

[17] M. Stumpf, "Pulsed EM field radiation, mutual coupling, and reciprocity of thin planar antennas," *IEEE Trans. Antennas Propag.*, vol. 62, no. 8, pp. 3943–3950, Aug. 2014.

[18] A. Shlivinski, "Time-domain transfer coupled response of antennas—Reciprocity theorem approach," *IEEE Trans. Antennas Propag.*, vol. 65, no. 4, pp. 1714–1727, Apr. 2017.

[19] Q. Wu and W. Su, "Rigorous eigenmode analysis of conducting sphere," presented at the Eur. Conf. Antennas Propag. (EuCAP), Lisbon, Portugal, 2015, pp. 1–4.

[20] M. Tsiklauri, N. Dikhaminjia, J. Fan, J. Drewniak, and M. Zvonkin, "Front delay based causality for network parameters," in *Proc. Asia–Pac. Int. Symp. Electromagn. Compat. (APEMC)*, Shenzhen, China, 2016, pp. 870–872.

[21] C. Yang, H. D. Brüns, P. Liu, and C. Schuster, "Impulse response optimization of band-limited frequency data for hybrid field-circuit simulation of large-scale energy-selective diode grids," *IEEE Trans. Electromagn. Compat.*, vol. 58, no. 4, pp. 1072–1080, Aug. 2016.

[22] K. Schab and J. Adams, "Modal decomposition of transients in direct antenna modulation systems," presented at the Eur. Conf. Antennas. Propag. (EuCAP), London, U.K., 2018, Art. no. CS08.5.

[23] M. Cabedo-Fabrés, A. Valero-Nogueira, J. I. Herranz-Herruzo, and M. Ferrando-Bataller, "A discussion on the characteristic mode theory limitations and its improvement for the effective modeling of antennas and arrays," in *Proc. IEEE Int. Symp. Antennas Propag. Soc.*, vol. 1. Monterey, CA, USA, 2004, pp. 121–124.

[24] A. V. Oppenheim, A. S. Willsky, and S. H. Nawab, *Signals and Systems*, 2nd ed. London, U.K.: Prentice-Hall, 1997, ch. 5.

[25] H. Bagci, A. E. Yilmaz, J.-M. Jin, and E. Michielssen, "Fast and rigorous analysis of EMC/EMI phenomena on electrically large and complex cable-loaded structures," *IEEE Trans. Electromagn. Compat.*, vol. 49, no. 2, pp. 361–381, May 2007.

[26] S. D. Corey and A. T. Yang, "Interconnect characterization using time-domain reflectometry," *IEEE Trans. Microw. Theory Techn.*, vol. 43, no. 9, pp. 2141–2156, Sep. 1995.

[27] C.-W. Hsue and T.-W. Pan, "Reconstruction of nonuniform transmission lines from time-domain reflectometry," *IEEE Trans. Microw. Theory Techn.*, vol. 45, no. 1, pp. 32–38, Jan. 1997.
[28] A. Cozza and L. Pichon, "Echo response of faults in transmission lines: Models and limitations to fault detection," *IEEE Trans. Microw. Theory Techn.*, vol. 64, no. 12, pp. 4155–4164, Dec. 2016.
[29] C. R. Paul, "A comparison of the contributions of common-mode and differential-mode currents in radiated emissions," *IEEE Trans. Electromagn. Compat.*, vol. 31, no. 2, pp. 189–193, May 1989.
[30] Z. Wen and Q. Wu, "Modal decomposition of transient responses in wireless power transfer system," in *Proc. 11th Int. Conf. Microw. Millimeter Wave Technol. (ICMMT)*, Guangzhou, China, 2019, pp. 1–3.
[31] K. Na, H. Jang, H. Ma, and F. Bien, "Tracking optimal efficiency of magnetic resonance wireless power transfer system for biomedical capsule endoscopy," *IEEE Trans. Microw. Theory Techn.*, vol. 63, no. 1, pp. 295–304, Jan. 2015.

QI WU (Member, IEEE) received the B.S. degree in electrical engineering from East China Normal University, Shanghai, China, in 2004, and the Ph.D. degree from Shanghai Jiao Tong University, Shanghai, in 2009.

He joined the faculty of School of Electronics and Information Engineering, Beihang University, Beijing, China, in 2009, where he is currently a Full Professor. From 2011 to 2012, he was a Visiting Scholar with the Department of Electrical Engineering, University of California, Los Angeles. From 2014 to 2016, he was an Alexander von Humboldt Fellow with the Institute of Electromagnetic Theory, Technical University of Hamburg, Germany. He has authored over 40 journal papers, two books, and holds ten Chinese patents and two U.S. patents as the first inventor. His research interests include broadband antennas, computational electromagnetics, and related EMC topics.

Prof. Wu received the Young Scientist Award from the International Union of Radio Science (URSI) in 2011, the Nominee Award for Excellent Doctoral Dissertation from the National Minister of Education in 2012, the Natural Science Award from Shanghai Government in 2013, the Young Scientist Award of APEMC in 2016, and the Supervisor for Excellent Master Thesis from Chinese institute of Electronics in 2018.

ZHONGKUI WEN received the B.S. and M.S. degrees in electrical engineering from Beihang University, Beijing, China, in 2016 and 2019, respectively.

In 2018, he was a visiting student with the Institute of Theoretical Electromagnetics, Hamburg University of Technology, Hamburg, Germany, for six months. He is currently an Engineer with Xiaomi Technology, Beijing. His research interests include the characteristic mode analysis and wireless power transfer.